学位論文(要約)

An evaluation of the direct aerosol radiative forcing from satellite remote sensing and climate modeling

(衛星リモートセンシングと気候モデルによるエアロゾル直接放射強制力の評価)

平成 26 年 12 月　博士(理学)申請

東京大学大学院理学系研究科

地球惑星科学専攻

及川　栄治

Abstract

Anthropogenic and natural aerosols affect the Earth's radiation budget both in direct and indirect way. The direct aerosol effect on Earth's radiation budget is caused by direct scattering and absorption of solar and thermal radiation, and can be quantified by the radiative forcing. In this study, shortwave direct aerosol radiative forcing (SWDARF) is estimated by using satellite observation data and climate modeling, and the uncertainties of estimated SWDARF are discussed.

In 2006, the Cloud-Aerosol Lidar and Infrared Pathfinder Satellite Observations (CALIPSO) satellite was launched with the space-borne lidar, CALIOP (the Cloud-Aerosol Lidar with Orthogonal Polarization). CALIOP, for the first time, provides us with a global data of aerosol and cloud vertical profiles [*Winker et al.*, 2009, 2013]. In addition, CALIOP has capability to detect aerosols existing above the optically thick clouds which are not observed by passive remote sensing and ground based lidar [*Winker et al.*, 2010]. Several studies reported that absorbing aerosols above low-level clouds produce a large positive forcing over the Atlantic Ocean off southwest Africa [e.g. *Keil and Haywood*, 2003; *Chand et al.*, 2009]. SWDARFs of aerosols above clouds have never been estimated in the global scale using observation data.

I investigate four scenarios for estimating the SWDARF at the top of the atmosphere (TOA) using data of CALIPSO lidar and data of MODIS sensor. The first scenario, which is called as clear-sky case, is the case that aerosols are observed in clear-sky condition. High cloud reflectance changes the SWDARF from negative to positive [*Haywood and Shine*, 1997]. Hence, I made three scenarios under cloudy-sky condition. The first is a case of aerosols existing above clouds (above-cloud case). The second is a case of aerosols existing below high-level clouds such as cirrus (below-cloud case). The third is a case of aerosols undetected by CALIOP lidar exist below/within the optically thick clouds (cloudy-undetected case). The cloudy-sky SWDARF is calculated by SWDARFs of above-cloud, below-cloud, and cloudy-undetected cases weighted by the occurrence probability of each scenario. The all-sky SWDARF is then calculated by combination of clear-sky and cloudy-sky SWDARF weighted by the cloud occurrence probability. In this study, the global scale estimate of cloudy-sky SWDARF is performed for the first time by using observation data. My analysis of the CALIPSO Version 3 product shows the occurrence probabilities in clear-sky, above-cloud, below-cloud, and cloudy-undetected cases are 38%, 4%, 16%, and 42%, respectively. This indicates that CALIOP can observe 58% of aerosols in all-sky condition, whereas the aerosol observation by passive remote sensing is limited only in clear-sky condition,

i.e. 38% of aerosols.

In clear-sky and below-cloud cases, aerosols mainly scatter sunlight and SWDARF shows negative values, except for bright surfaces. On the other hand, SWDARF globally shows positive value in above-cloud case. In this case, the absorption of aerosols is enhanced by the high reflectance of clouds and changes the SWDARF at TOA from negative to positive. As for the cloudy-undetected case, I assume the SWDARF to be zero, because optically thick clouds dominantly scatter the incident sunlight. The above mentioned method of analysis is applied to CALIPSO Version 2 and Version 3 products to obtain SWDARFs between 60°S and 60°N under clear-sky, cloudy-sky, and all-sky conditions as −3.7±0.8, −3.7±0.7, and −2.0±1.2 Wm^{-2}. The result indicates the difference of the version of the CALIPSO product is as large as 50% in all-sky forcing.

According to previous studies of the global aerosol model intercomparison project AeroCom, SWDARF simulated by MIROC-SPRINTARS is smaller negative than the mean value of other model estimates [*Yu et al.*, 2006; *Schulz et al.*, 2006; *Myhre et al.*, 2013]. In this study, SWDARF is also calculated by the latest version of MIROC [*Watanabe et al.*, 2010]. In the MIROC model, the optical properties of aerosols and clouds are separately calculated in SPRINTARS aerosol module and mstrnX radiation module. By detailed investigation of aerosol optical thickness (AOT) and and single scattering albedo (SSA) from the two modules, I found that the mstrnX AOT and SSA are smaller than those of SPRINTARS, because aerosol size indices of mstrnX is different from that of SPRINTARS in order to save CPU time. In order to make the two modules consistent with each other, I modified the interface between the two modules to set common optical aerosol models with 6 size bins of mineral dust, 4 types of carbonaceous aerosols, sulfate, and 4 size bins of sea salt. In this study, this new model is referred to as the SPnew model. I confirmed that AOT of each aerosol component and SSA of mstrnX agree with those of SPRINTARS within 4% in the SPnew model. Absorption of dust and carbonaceous aerosols becomes smaller from the standard model to the SPnew model. Zonal averages of SWDARF between 60°S and 60°N under clear-sky, cloudy-sky, and all-sky conditions change from −2.0, +0.3, and −0.7 Wm^{-2} in the standard model to −2.1, −0.1, and −1.1 Wm^{-2} in SPnew model.

The vertical profiles of aerosols are globally observed by CALIPSO lidar under clear-sky condition. High concentrated aerosols are globally observed by CALIPSO lower than 2 km altitude; in particular, aerosol extinction coefficient is larger than 0.05 at altitude lower than 1 km. On the other hand, the aerosol extinction coefficient in SPnew model is underestimated globally below 2 km altitude, while aerosols are elevated up to 7 km altitude around source regions of carbonaceous aerosols and dust in the model. These results indicate that aerosols are transported higher than the observation in a vertical direction, but are hardly transported in a horizontal direction in MIROC.

I compared the the obtained geographical distributions of AOT and SSA from satellites and models. The geographical distribution of CALIPSO AOT is found similar to that of MODIS observations, while CALIPSO AOT is smaller than MODIS AOT by 20%. Compared with CALIPSO and MODIS AOT, SPnew AOT is underestimated in almost all regions. This causes smaller negative SWDARF under clear-sky condition in the model. It is also found that under clear-sky condition the aerosol extinction coefficient of SPnew is smaller below 4 km altitude and larger above 4 km altitude than that of CALIPSO. The ratio of CALIPSO AOT to SPnew AOT (CALIPSO AOT / SPnew AOT) is 2.14 below 4 km and 0.29 above 4 km altitude. In order to study the effect of this difference, I performed a model simulation that aerosol concentrations multiplied by 2.14 below 4 km altitude and 0.29 above 4 km altitude in the SPnew model. This simulation is referred to as the SP4km experiment.

Zonal averages of SWDARF between 60°S and 60°N under clear-sky, cloudy-sky, and all-sky conditions are calculated in the SP4km experiment as −3.2, -0.3, and −1.7 Wm^{-2}. The zonal average AOT between 60°S and 60°N for SP4km is comparable to CALIPSO AOT and the modeled SSA is overestimated, but the zonal average of clear-sky SWDARF for SP4km is smaller negative than CALIPSO by 0.5 Wm^{-2}. This difference is mainly caused by an underestimation of aerosol extinction coefficient below 2 km altitude over ocean in the Southern Hemisphere.

MIROC frequently simulate optically thicker clouds than observation. Off southwest Africa, absorbing aerosols emitted by biomass burning in Africa are transported above low-level clouds. Aerosols usually undetected below 1.5 km altitude by CALIPSO observations in above-cloud case, whereas aerosols are simulated from surface to 5 km altitude in the model. In cloudy-sky condition, the modeled SWDARF is more positive than the observation, because the absorption of aerosols within/above clouds is largely enhanced by higher cloud reflectance derived from optically thick clouds. Over central and northern Pacific, optically thick clouds are simulated from the lower to upper troposphere in the model, so that clouds mainly scatter sunlight and aerosols cause less negative forcing than the CALIPSO case. From these results, the cloudy-sky SWDARF in MIROC is considered to be smaller negative than that of CALIPSO.

Summarizing the results in this study, I like to propose the best estimates of clear-sky and all-sky SWDARF of −4.1 and −1.9 Wm^{-2}. On the other hand, the global averages of SWDARF from the past studies are -4.8 ± 0.8 and -2.7 ± 0.9 Wm^{-2} under clear-sky and all-sky conditions [*Liu et al*., 2007; *Kim and Ramanathan,* 2008; *Ma et al.,* 2012; *Zhang et al.,* 2012; *Kinne et al.,* 2013]. My estimate of the clear-sky SWDARF is located in between the CALIPSO values obtained in this study and the average of previous studies. This conclusion suggests that both the satellite-borne lidar and modeling methods have their own characteristic errors in SWDARF estimation. The present analysis is considered to be useful to identify causes for errors found in this study.

Contents

1. Introduction

Dust, sea salt, and volcanic sulfate are naturally emitted to the atmosphere as natural aerosols. Major sources of anthropogenic aerosols are, on the other hand, fossil fuel, biofuel, and biomass burning. Most of current global aerosol models treat natural aerosols, anthropogenic sulfate, black carbon (BC), and organic carbon (OC). Some models simulate these species and anthropogenic nitrate and secondary organic aerosols (SOA). Anthropogenic and natural aerosols affect the Earth's radiation budget both directly and indirectly. The direct aerosol effect is caused by direct scattering and absorption of solar and thermal radiation. The indirect aerosol effect is caused by the influence of aerosols that change the cloud microphysical and optical properties and also the cloud amount and lifetime by acting as cloud condensation nuclei (CCN) [*Twomey*, 1977; *Albrecht*, 1989]. Moreover, absorption of solar radiation by aerosols can influence the atmospheric temperature structure and lead to evaporation of cloud droplets. This phenomenon is called the semi-direct aerosol effect [*Hansen et al*., 1997; *Ackerman et al*., 2000].

In this study, I focus on the direct aerosol effect, which can be quantified by the radiative forcing. Under all-sky condition, direct aerosol radiative forcing (DARF) of anthropogenic aerosols has been estimated by various global models as -0.35 ± 0.5 Wm^{-2} [*IPCC,* 2013]. The Aerosol interComparison project AeroCom (http://nansen.ipsl.jussieu.fr/AEROCOM) attempts to the understanding of global aerosol life cycle and its impact on climate by performing a systematic analysis of more than 16 different global aerosol model results in addition to a comparison with satellite and surface measurements [e.g., *Kinne et al.*, 2006; *Textor et al*., 2006; *Schulz et al.*, 2006; *Myhre et al*., 2013]. DARF reported in *IPCC* [2013] was mainly based on the DARF simulated by the AeroCom models [*Myhre et al*., 2013]. AeroCom 16 models simulated the clear-sky and all-sky DARF of anthropogenic aerosols and resulted in mean values of −0.65 Wm^{-2} and −0.27 Wm^{-2} in clear-sky and all-sky conditions, respectively. The range of clear-sky DARF was from −0.35 to −1.01 Wm^{-2} and that of all-sky DARF was −0.58 to −0.02 Wm^{-2}. Several models did not include nitrate or SOA for the simulation. A correction of the model estimates for missing aerosol components leaded the mean all-sky DARF to be −0.35 Wm^{-2}. There are still large uncertainties in DARF calculated by various global aerosol models that estimate the climate effects by aerosols.

Total (natural and anthropogenic) aerosols are observed by ground-based and satellite-based measurements. AERosol RObotic NETwork (AERONET) [*Holben et al.*, 1998] and SKYNET [*Nakajima et al.*, 1996] are the world-wide ground-based observation networks to retrieve aerosol parameters (aerosol optical thickness (AOT), single scattering albedo (SSA), the complex refractive index, and the size and shape distributions from spectral and multiangular sun/sky radiometer observations. Although the high-quality observations come from ground-based observations, satellite observations cover the land and ocean on a global scale. Especially, aerosol observations by the Moderate Resolution Imaging Spectroradiometer (MODIS) sensors aboard the Aqua and Terra satellites are well-known [e.g., *Remer et al.*, 2005, 2008]. Validation of MODIS observations was conducted using AERONET observations over both land and ocean [e.g., *Chu et al.*, 2002; *Ichoku et al.*, 2002; *Remer et al.*, 2002]. Assumed retrieved errors of MODIS AOT are $\Delta\tau = \pm(0.03 + 0.05\tau)$ over ocean, and $\Delta\tau = \pm(0.05 + 0.15\tau)$ over land, where τ represents AOT [*Remer et al.*, 2005, 2008]. *Remer et al.* [2008] reported that the multiannual global averages of AOT at 550 nm over ocean were 0.13 for Aqua and 0.14 for Terra, and those over land were 0.19 for both Aqua and Terra; however, AOT over the bright surfaces (deserts and snow and ice surfaces) is not retrieved by using the dark target approach, because the observed radiance is dominated by the surface reflectance. It should be noted that the land AOT is the averages over the land except for desert regions and cryosphere.

Recent studies about the clear-sky shortwave DARF (SWDARF) of total aerosols at the top-of-atmosphere (TOA) were summarized in *Yu et al.* [2006]. The satellite-based SWDARF was estimated to be -5.3 ± 0.2 Wm^{-2} and the model-based SWDARF was -3.3 ± 0.6 Wm^{-2}. The difference of SWDARF between observations and models were larger than the standard errors of observed and modeled SWDARFs. It is said that the MODIS-retrieved AOT tends to be overestimated by about 10 to 15%, because of contamination of thin cirrus [*Kaufman et al.*, 2005]. Such overestimation of AOT would result in a comparable overestimate of SWDARF. The modeled SWDARF was smaller than the measurement-based SWDARF by about 30 to 40%, even after accounting for a cloud contamination.

The global mean DARF at the TOA for anthropogenic and total aerosols were summarized in Fig. 1-1. On the global scale, aerosols mainly cool the Earth by reflecting sunlight back to space, that is, aerosols cause a negative forcing. The magnitude of the negative forcing for total aerosols is several times greater than that for anthropogenic aerosols. One of global aerosol models that have participated in AeroCom project is called Spectral Radiation-Transport Model for Aerosol Species (SPRINTARS) [*Takemura et al.*, 2000, 2005, 2009]. The DARFs calculated by SPRINTARS are also summarized in Fig. 1-1. SPRINTARS simulated −0.71 and −0.14 Wm^{-2} for the clear-sky and all-sky DARFs of anthropogenic aerosols, respectively. The clear-sky forcing was comparable to the model average, while the all-sky forcing was a half the value of the model average. It could be that since nitrate and SOA were not included in SPRINTARS simulation. In view of different aerosol components simulated in different models, the SPRRINTARS all-sky forcing became close to the model average; however, the SPRINTARS clear-sky forcing became largely different from the model average. The clear-sky DARF for total aerosols was also simulated by SPRINTARS in the model and observation comparison exercises [*Yu et al.*, 2006]. The clear-sky DARF of SPRINTARS was −1.7 Wm^{-2}; even allowing for missing aerosol components, the SPRINTARS DARF for total aerosols was smaller than DARFs by other studies.

One of uncertainties in the evaluated DARF is the effect of vertical stratification of aerosols and clouds. Previous studies suggested that the all-sky DARF significantly depends on the amount of aerosols loaded above the cloud layer. In particular, absorbing aerosols as emitted from biomass burning above clouds produce a large positive forcing off southern Africa and South America [*Keil and Haywood*, 2003; *Takemura et al.*, 2005]. *Haywood et al.* [2004] used the vertical profiles of aerosols and clouds off the coast of southern Africa from aircraft measurements to demonstrate that MODIS retrievals exhibit a low bias in the cloud optical thickness (COT) and cloud effective radius. *De Graaf et al.* [2012] used data of passive satellite spectrometry from the ultraviolet to the shortwave infrared for estimating aerosol solar absorption by the above-cloud aerosols. The cloud optical properties were retrieved using three channels in shortwave infrared for calculating the cloud reflectance in the modeled aerosol-free condition. SWDARF was estimated by the difference of the cloud reflectance between measurements and modeled aerosol-free calculations. They reported that SWDARF of above-cloud absorbing aerosols off southern Africa was +23 Wm^{-2} in August 2006.

In 2006, the Cloud-Aerosol Lidar and Infrared Pathfinder Satellite Observations (CALIPSO) satellite was launched with the space-borne lidar, CALIOP (the Cloud-Aerosol Lidar with Orthogonal Polarization), as one of the NASA Earth System Science Pathfinder (ESSP) programs. CALIOP, for the first time, provided us with global data of aerosol and cloud vertical profiles [*Winker et al.*, 2009, 2013]. Clouds and aerosols were discriminated using a combination of 532 nm backscatter magnitude and attenuated color ratio, which is the ratio of 1064 to 532 nm of attenuated backscatter intensity [*Liu et al.*, 2009]. Vertical profiles of extinction coefficients for clouds and aerosols were retrieved from the extinction retrieval algorithms [*Young and Vaughan*, 2009]. *Winker et al.*, [2013] showed some aerosol characteristics retrieved by the CALIPSO measurements. In most regions, clear-sky and all-sky mean extinction profiles for aerosols were similar; it implied that aerosol loadings in the lower troposphere are uncorrelated with the occurrence of high-level clouds. Diurnal differences of the column AOT was larger over land than over ocean. In addition, CALIOP can detect and retrieve aerosols above clouds [*Winker et al*., 2010], while these aerosols are undetected from ground-based lidar measurements. *Chand et al.* [2009] evaluated the direct aerosol effect over the Atlantic Ocean off southwest Africa using AOT of aerosols above optically thick low-level clouds quantified by retrieval methods of *Hu et al.* [2007] and *Chand et al.* [2008]. *Chand et al.* [2009] reported that the DARF largely depends on the fractional coverage and albedo of the underlying clouds: thus, cloud and aerosol profiling is significantly important for an accurate evaluation of the direct aerosol effect.

In this study, the global all-sky SWDARF of the total (natural plus anthropogenic) aerosols is calculated using aerosol and cloud distributions of both CALIPSO observations and global aerosol modeling with SPRINTARS [*Takemura et al*., 2000, 2005, 2009] for discussing the uncertainties of estimation of SWDARF from observations and models. Distributions of aerosols and clouds from CALIPSO and MODIS observations and satellite-based SWDARF are shown in chapter 2. I present a new method of improving aerosol optical modeling in the SPRINTARS and the radiation code in chapter 3. Comparisons between observations and model simulations are made in chapter 4 to study the sensitivity of the model simulation to the assumed aerosol characteristics. The overall results are summarized and discussed in chapter 5.

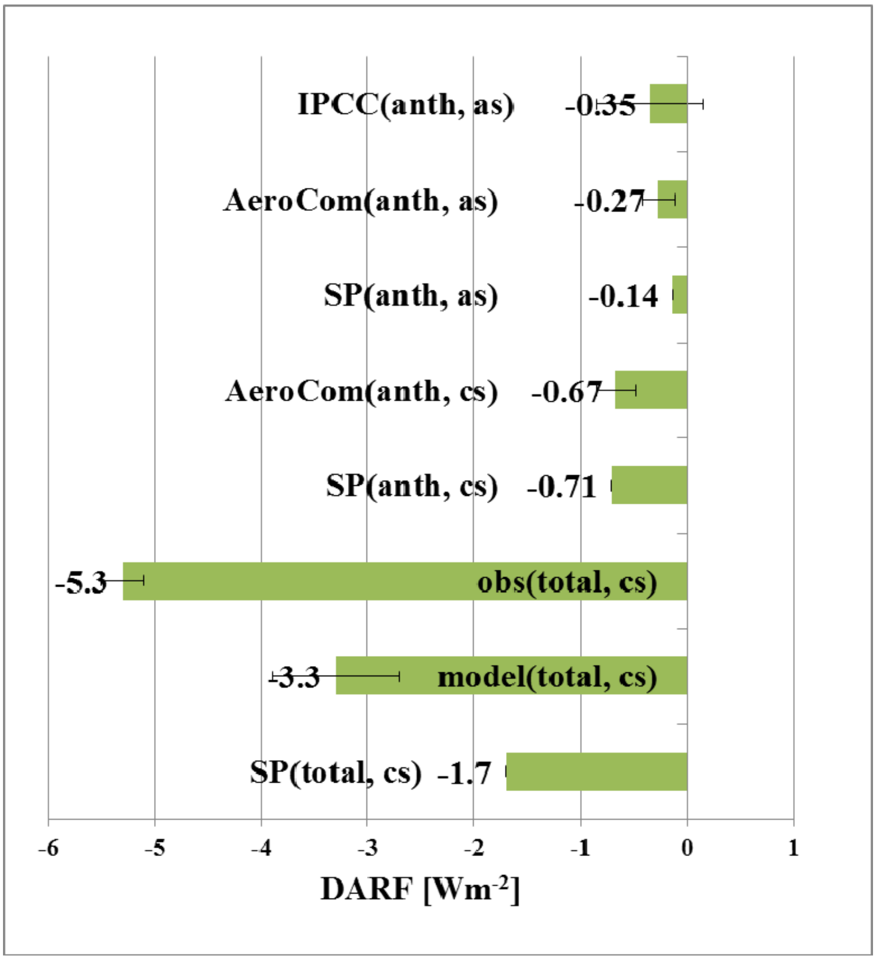

Fig. 1-1. Direct aerosol radiative forcing (DARF) at the top of atmosphere for anthropogenic and total (anthropogenic+natural) aerosols. Data of the all-sky and clear-sky DARF for anthropogenic aerosols ((anth, as) and (anth, cs)) are referred to *IPCC* [2013] and the simulation results of the AeroCom models (AeroCom) and SPRINTARS model (SP) [*Myhre et al*., 2013]. The clear-sky DARFs for total aerosols (total, cs) are estimated by the multi-satellite observations (obs) and multi-models (model) and SPRINTARS model [*Yu et al*., 2006].

2. Direct aerosol radiative forcing of CALIPSO satellite measurements

This chapter is non-public, because the contents of this chapter will be published within 4 years.

3. Direct aerosol radiative forcing of AGCM

This chapter is non-public, because the contents of this chapter will be published within 4 years.

4. Comparison between the observation and model results

This chapter is non-public, because the contents of this chapter will be published within 4 years.

5. Summary

In this study, shortwave direct aerosol radiative forcing (SWDARF) is estimated by using satellite observation data and climate modeling, and the uncertainties of estimated SWDARF are discussed.

The CALIPSO satellite with CALIOP lidar, for the first time, provides us with a global data of aerosol and cloud vertical profiles [*Winker et al*., 2009, 2013]. In addition, CALIOP has capability to detect aerosols existing above the optically thick clouds which are not observed by passive remote sensing and ground based lidar [*Winker et al*., 2010]. Several studies reported that absorbing aerosols above low-level clouds produce a large positive forcing over the Atlantic Ocean off southwest Africa [e.g. *Keil and Haywood*, 2003; *Chand et al*., 2009]. SWDARFs of aerosols above clouds have never been estimated in the global scale using observation data.

I investigate four scenarios for estimating the SWDARF at the top of the atmosphere (TOA) using data of CALIPSO lidar and data of MODIS sensor. The first scenario is a case that aerosols are observed in clear-sky condition (clear-sky case). The second scenario is a case of aerosols existing above clouds (above-cloud case). The third scenario is a case of aerosols existing below high-level clouds such as cirrus (below-cloud case). The fourth scenario is a case of aerosols undetected by CALIOP lidar exist below/within the optically thick clouds (cloudy-undetected case). The cloudy-sky SWDARF is calculated by SWDARFs of above-cloud, below-cloud, and cloudy-undetected cases weighted by the occurrence probability of each scenario. The all-sky SWDARF is then calculated by combination of clear-sky and cloudy-sky SWDARF weighted by the cloud occurrence probability. In this study, the global scale estimate of cloudy-sky SWDARF is performed for the first time by using observation data. My analysis of the CALIPSO Version 3 product shows the occurrence probabilities in clear-sky, above-cloud, below-cloud, and cloudy-undetected cases are 38%, 4%, 16%, and 42%, respectively. This indicates that CALIOP can observe 58% of aerosols in all-sky condition, whereas the aerosol observation by passive remote sensing is limited only in clear-sky condition, i.e. 38% of aerosols.

In clear-sky and below-cloud cases, aerosols mainly scatter sunlight and SWDARF shows negative values, except for bright surfaces. On the other hand, SWDARF globally shows positive value in above-cloud case. In this case, the absorption of aerosols is enhanced by the high reflectance of clouds and changes the SWDARF at TOA from negative to positive. As for the cloudy-undetected case, I assume the SWDARF to be zero, because optically thick clouds dominantly scatter the incident sunlight. The above mentioned method of analysis is applied to CALIPSO Version 2 and Version 3 products to obtain SWDARFs between 60°S and 60°N under clear-sky, cloudy-sky, and all-sky conditions as −3.7±0.8, −3.7±0.7, and −2.0±1.2 Wm^{-2}. The result indicates the difference of the version of the CALIPSO product is as large as 50% in all-sky forcing.

According to previous studies of the global aerosol model intercomparison project AeroCom, SWDARF simulated by MIROC-SPRINTARS is smaller negative than the mean value of other model estimates [*Yu et al.*, 2006; *Schulz et al.*, 2006; *Myhre et al.*, 2013]. In this study, SWDARF is also calculated by the latest version of MIROC [*Watanabe et al.*, 2010]. In the MIROC model, the optical properties of aerosols and clouds are separately calculated in SPRINTARS aerosol module and mstrnX radiation module. By detailed investigation of aerosol optical thickness (AOT) and and single scattering albedo (SSA) from the two modules, I found that the mstrnX AOT and SSA are smaller than those of SPRINTARS, because aerosol size indices of mstrnX is different from that of SPRINTARS in order to save CPU time. In order to make the two modules consistent with each other, I modified the interface between the two modules to set common optical aerosol models with 6 size bins of mineral dust, 4 types of carbonaceous aerosols, sulfate, and 4 size bins of sea salt. In this study, this new model is referred to as the SPnew model. I confirmed that AOT of each aerosol component and SSA of mstrnX agree with those of SPRINTARS within 4% in the SPnew model. Absorption of dust and carbonaceous aerosols becomes smaller from the standard model to the SPnew model. Zonal averages of SWDARF between 60°S and 60°N under clear-sky, cloudy-sky, and all-sky conditions change from −2.0, +0.3, and −0.7 Wm^{-2} in the standard model to −2.1, −0.1, and −1.1 Wm^{-2} in SPnew model.

The vertical profiles of aerosols are globally observed by CALIPSO lidar under clear-sky condition. High concentrated aerosols are globally observed by CALIPSO lower than 2 km altitude; in particular, aerosol extinction coefficient is larger than 0.05 at altitude lower than 1 km. On the other hand, the aerosol extinction coefficient in SPnew model is underestimated globally below 2 km altitude, while aerosols are elevated up to 7 km altitude around source regions of carbonaceous aerosols and dust in the model. These results indicate that aerosols are transported higher than the observation in a vertical direction, but are hardly transported in a horizontal direction in MIROC.

I compared the the obtained geographical distributions of AOT and SSA from satellites and models. The geographical distribution of CALIPSO AOT is found similar to that of MODIS observations, while CALIPSO AOT is smaller than MODIS AOT by 20%. Compared with CALIPSO and MODIS AOT, SPnew AOT is underestimated in almost all regions. This causes smaller negative SWDARF under clear-sky condition in the model. It is also found that under clear-sky condition the aerosol extinction coefficient of SPnew is smaller below 4 km altitude and larger above 4 km altitude than that of CALIPSO. The ratio of CALIPSO AOT to SPnew AOT (CALIPSO AOT / SPnew AOT) is 2.14 below 4 km and 0.29 above 4 km altitude. In order to study the effect of this difference, I performed a model simulation that aerosol concentrations multiplied by 2.14 below 4 km altitude and 0.29 above 4 km altitude in the SPnew model. This simulation is referred to as the SP4km experiment.

Zonal averages of SWDARF between 60°S and 60°N under clear-sky, cloudy-sky, and all-sky conditions are calculated in the SP4km experiment as −3.2, -0.3, and −1.7 Wm^{-2}. The zonal average AOT between 60°S and 60°N for SP4km is comparable to CALIPSO AOT and the modeled SSA is overestimated, but the zonal average of clear-sky SWDARF for SP4km is smaller negative than CALIPSO by 0.5 Wm^{-2}. This difference is mainly caused by an underestimation of aerosol extinction coefficient below 2 km altitude over ocean in the Southern Hemisphere.

MIROC frequently simulate optically thicker clouds than observation. Off southwest Africa, absorbing aerosols emitted by biomass burning in Africa are transported above low-level clouds. Aerosols usually undetected below 1.5 km altitude by CALIPSO observations in above-cloud case, whereas aerosols are simulated from surface to 5 km altitude in the model. In cloudy-sky condition, the modeled SWDARF is more positive than the observation, because the absorption of aerosols within/above clouds is largely enhanced by higher cloud reflectance derived from optically thick clouds. Over central and northern Pacific, optically thick clouds are simulated from the lower to upper troposphere in the model, so that clouds mainly scatter sunlight and aerosols cause less negative forcing than the CALIPSO case. From these results, the cloudy-sky SWDARF in MIROC is considered to be smaller negative than that of CALIPSO.

Summarizing the results in this study, I like to propose the best estimates of clear-sky and all-sky SWDARF of −4.1 and −1.9 Wm^{-2}. On the other hand, the global averages of SWDARF from the past studies are −4.8±0.8 and −2.7±0.9 Wm^{-2} under clear-sky and all-sky conditions [*Liu et al*., 2007; *Kim and Ramanathan,* 2008; *Ma et al.,* 2012; *Zhang et al.,* 2012; *Kinne et al.,* 2013]. My estimate of the clear-sky SWDARF is located in between the CALIPSO values obtained in this study and the average of previous studies. This conclusion suggests that both the satellite-borne lidar and modeling methods have their own characteristic errors in SWDARF estimation. The present analysis is considered to be useful to identify causes for errors found in this study.

Appendix A

In this study, four scenarios for radiative transfer calculation in CALIPSO observations, *i.e.* clear-sky, above-cloud, below-cloud, and cloudy-undetected cases, are investigated. The conditional occurrence probability of aerosols observed in the clear-sky condition is given as

$$P_a = \frac{N_a}{N_{\text{clear-sky}}}, \tag{A-1}$$

where N_a is the pixel count where aerosols are observed in clear-sky condition and $N_{\text{clear-sky}}$ is the pixel count in clear-sky condition. We use the conditional AOT at wavelength of 532 nm for radiative transfer calculations defined as

$$\tau_a = \frac{\tau_{a,sum}}{N_a}, \tag{A-2}$$

where $\tau_{a,sum}$ is the sum of AOT observed at clear-sky pixels. The clear-sky AOT shown in Fig. 2-8 is given as

$$\tau_{\text{clear-sky}} = \frac{\tau_{a,sum}}{N_{\text{clear-sky}}} = P_a \frac{\tau_{a,sum}}{N_{\text{a}}}. \tag{A-3}$$

Shortwave direct aerosol radiative forcing (SWDARF) in clear-sky case is defined as

$$SWDARF_{\text{clear-sky}} = P_a \times SWDARF_a, \tag{A-4}$$

where $SWDARF_a$ is the SWDARF calculated by using τ_a.

In a similar way, P_{ac}, P_{bc}, and P_{uc} are the conditional occurrence probabilities of above-cloud, below-cloud, and cloudy-undetected cases, respectively:

$$P_{ac} = \frac{N_{ac}}{N_{\text{cloudy-sky}}}, \quad P_{bc} = \frac{N_{bc}}{N_{\text{cloudy-sky}}}, \quad \text{and} \quad P_{uc} = \frac{N_{\text{cloudy-sky}} - N_{ac} - N_{bc}}{N_{\text{cloudy-sky}}}, \tag{A-5}$$

$$P_{ac} + P_{bc} + P_{uc} = 1, \tag{A-6}$$

where N_{ac}, N_{bc}, and $N_{\text{cloudy-sky}}$ are the pixel counts of above-cloud, below-cloud and cloudy-sky cases, respectively. τ_{ac} and τ_{bc} are AOTs for radiation calculations in above-cloud and below-cloud cases, respectively:

$$\tau_{ac} = \frac{\tau_{ac,sum}}{N_{ac}} \quad \text{and} \quad \tau_{bc} = \frac{\tau_{bc,sum}}{N_{bc}} \tag{A-7}$$

where $\tau_{ac,sum}$ and $\tau_{bc,sum}$ are the sums of AOT observed in above-cloud and below-cloud cases, respectively. The cloudy-sky AOT is given as

$$\tau_{\text{cloudy-sky}} = \frac{\sum_{i=ac,bc,uc} \tau_{i,sum}}{N_{cloudysky}} = \sum_{i=ac,bc} P_i \cdot \tau_i + 0 = \sum_{i=ac,bc} P_i \cdot \tau_i. \tag{A-8}$$

The SWDARF in cloudy-sky condition is then given as

$$\begin{aligned} SWDARF_{\text{cloudy-sky}} &= \sum_{i=ac,bc,uc} P_i \times SWDARF_i \\ &\approx \sum_{i=ac,bc} P_i \times SWDARF_i + 0 = \sum_{i=ac,bc} P_i \times SWDARF_i \end{aligned} . \tag{A-9}$$

where SWDARF of the cloudy-undetected case is assumed to be close to zero, because optically thick clouds dominantly scatter the incident sunlight.

The AOT and SWDARF under all-sky condition are given as

$$\tau_{\text{all-sky}} = P_{\text{clear-sky}} \cdot \tau_{\text{clear-sky}} + P_{\text{cloudy-sky}} \cdot \tau_{\text{cloudy-sky}}, \tag{A-10}$$

$$SWDARF_{\text{all-sky}} = P_{\text{clear-sky}} \times SWDARF_{\text{clear-sky}} + P_{\text{cloudy-sky}} \times SWDARF_{\text{cloudy-sky}}, \tag{A-11}$$

where $P_{\text{cloudy-sky}}$ is equivalent to column cloud cover fraction, C.

Appendix B

The aerosol size distribution is usually expressed by the log-normal distribution and the number size distribution is expressed by

$$\frac{dN}{d\ln r} = \frac{C_n}{\sqrt{2\pi}\ln(\sigma_g)} \exp\left(-\frac{1}{2}\left(\frac{\ln(r/r_n)}{\ln(\sigma_g)}\right)^2\right), \tag{B-1}$$

where $dN/d\ln(r)$ is number of aerosol particles with radius in the infinitesimal size range $r \pm d\ln(r)$, r_n is number mean radius, C_n is total aerosol columnar particle number, and σ_g is geometric standard deviation (GSD) of the size distribution. The volume size distribution is

$$\frac{dV}{d\ln r} = \frac{C_v}{\sqrt{2\pi}\ln(\sigma_g)} \exp\left(-\frac{1}{2}\left(\frac{\ln(r/r_v)}{\ln(\sigma_g)}\right)^2\right), \tag{B-2}$$

where r_v is volume mean radius and C_v is total aerosol columnar particle volume. The relationship between r_v and r_n is expressed by

$$r_v = r_n \exp\left(3 \cdot \ln^2(\sigma_g)\right), \tag{B-3}$$

and the relationship between C_v and C_n is expressed by

$$C_v = \frac{4\pi}{3} r_n^3 \exp\left(4.5 \cdot \ln^2(\sigma_g)\right) C_n . \tag{B-4}$$

From equation B-4, the average mass of one aerosol particle m_p is given by

$$m_p = \frac{C_v}{C_n} \times m_a = \frac{4\pi}{3} r_n^3 \exp\left(4.5 \cdot \left(\ln(\sigma_g)\right)^2\right) m_a, \tag{B-5}$$

where m_a is mass per unit volume. Total aerosol columnar particle number N is given by

$$N = \frac{M_a}{m_p}, \tag{B-6}$$

where M_a is total aerosol columnar particle mass.

SPRINTARS treats 6 size bins of dust particle and 4 size bins of sea salt [*Takemura et al.*, 2009]. In SPnew model, aerosol volume size distribution in each size bin is defined by the log-normal distribution. Figures B-1 and B-2 show the log-normal distributions of dust and sea salt at each sizes based on Table 3-2. From these figures, GSDs of volume size distributions for dust and sea salt are set to 1.1 and 1.2 in SPnew model.

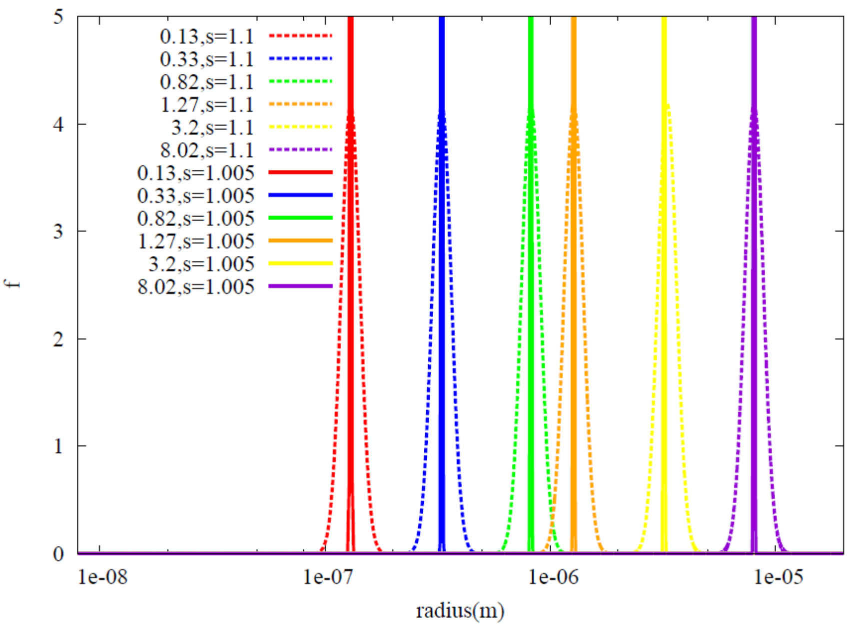

Fig. B-1. The log-normal distributions of 6 different size dust particles in the cases of GSD = 1.005 and GSD = 1.1.

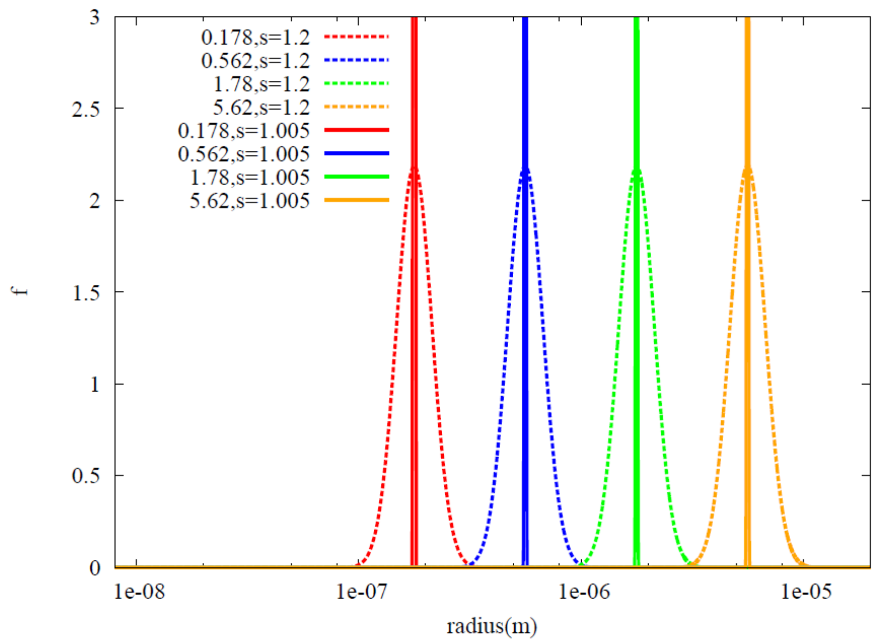

Fig. B-2. The log-normal distributions of 4 different size sea salt particles in the cases of GSD = 1.005 and GSD = 1.2.

Appendix C

I use AERONET Level 1.5 Product [*Holben et al.*, 1998; *Dubovik et al*., 2006] for the comparison of CALIPSO observation and MIROC model. AERONET Level 2 Product is the quality-assured products. The number of data in level 2 product is only 10% of that in level 1.5 product, so that AERONET level 1.5 product is used in this study. AERONET level 1.5 product includes a certain amount of data which has too large absorbing property ($\omega(\lambda) < 0.6$); therefore, a data selection procedure is performed to remove the low-quality data. I select the data which has $1.33 < m_r(\lambda) < 1.6$, $m_i(\lambda) < 0.1$, and $\omega(\lambda) < 0.987$, where m_r and m_i are the real part and imaginary part of refractive index, ω is SSA, and λ = 440, 675, 870, and 1020 nm. In addition, I eliminate the data which has both $\tau(\lambda) < 0.05$ and $FMF(\lambda) < 0.985$, where τ is AOT and FMF is fine mode fraction of AOT. After these data selections, SSA at 550 nm is interpolated using SSA at 440 and 675 nm. The calculated SSA at 550 nm is used for the comparison of CALIPSO observation and MIROC model (see section 4.3).

Acknowledgements

I am deeply grateful to Prof. Teruyuki Nakajima at Atmosphere and Ocean Research Institute (AORI), the University of Tokyo, for giving the notable subject of research and insightful comments during many years of the doctoral course for my study.

I am indebted to Asst. Prof. Miho Sekiguchi at Tokyo University of Marine Science and Technology for technical comments about the radiation models of Rstar, Fstar, and mstrnX. I would like to thank Dr. D. Goto at National Institute for Environmental Studies (NIES) for helping my research about the MIROC-AGCM simulation. I appreciate Dr. Nishizawa at NIES for his kind advice about the lidar observations. I have a lot to be thankful to Dr. Nick Schutgens, Dr. Toshiro Inoue, Dr. Haruo Tsuruta, and Dr. Junya Uchida for discussions and comments about my study.

I would also like to express my gratitude to my family for their moral support and warm encouragements.

The model simulations were performed by using the supercomputer system (NEC SX-9A/ECO) of the NIES.

References

Ackerman, A. S., O. B. Toon, D. E. Stevens, A. J. Heymsfield, V. Ramanathan, and E. J. Welton (2000), Reduction of tropical cloudiness by soot, *Science*, *288*, 1042-1047, doi:10.1126/science.288.5468.1042.

Albrecht, B. A. (1989), Aerosols, cloud microphysics, and fractional cloudiness, *Science*, *245*, 1227–1230.

d'Almeida, G. A., P. Koepke, and E. P. Shettle (1991), *Atmospheric Aerosols: Global Climatology and Radiative Characteristics*, A. Deepak Publishing, Hampton, VA.

Bellouin, N., A. Jones, J. Haywood, and S. A. Christopher (2008), Updated estimate of aerosol direct radiative forcing from satellite observations and comparison against the Hadley Centre climate model, *J. Geophys. Res.*, *113*, D10205, doi:10.1029/2007JD009385.

Bougamont, M., J. L. Bamber, and W. Greuell (2005), A surface mass balance model for the Greenland Ice Sheet, *J. Geophys. Res*., *110*, F04018, doi:10.1029/2005JF000348.

Chand, D., T. L. Anderson, R. Wood, R. J. Charlson, Y. Hu, Z. Liu, and M. Vaughan (2008), Quantifying above-cloud aerosol using spaceborne lidar for improved understanding of cloudy-sky direct climate forcing, *J. Geophys. Res.*, *113*, D13206, doi:10.1029/2007JD009433.

Chand, D., R. Wood, T. L. Anderson, S. K. Satheesh, and R. J. Charlson (2009), Satellite-derived direct radiative effect of aerosols dependent on cloud cover, *Nature Geoscience*, *2*, 181-184, doi:10.1038/NGE0437.

Chu, D. A., Y. J. Kaufman, C. Ichoku, L. A. Remer, D. Tanré, and B. N. Holben (2002), Validation of MODIS aerosol optical depth retrieval over land, *Geophys. Res. Lett.*, *29(12)*, doi:10.1029/2001GL013205.

Coddington, O. M., P. Pilewskie, J. Redemann, S. Platnick, P. B. Russell, K. S. Schmidt, W. J. Gore, J. Livingston, G. Wind, and T. Vukicevic (2010), Examining the impact of overlying aerosols on the retrieval of cloud optical properties from passive remote sensing, *J. Geophys. Res.*, *115*, D10211, doi:10.1029/2009JD012829.

De Graaf, M., L. G. Tilstra, P. Wang, and P. Stammes (2012), Retrieval of the aerosol direct radiative effect over clouds from spaceborne spectrometry, *J. Geophys. Res.*, *117*, D07207, doi:10.1029/2011JD017160.

Deepak, A. and H. G. Gerber (Eds.) (1983), Report of the experts meeting on aerosols and their climatic effects, World Meteorological Organization, Geneva, Switzerland, *Rep. WCP-55*, 107 pp.

Dubovik, O., B. Holben, T. F. Eck, A. Smirnov, Y. J. Kaufman, M. D. King, D. Tanré, and I. Slutsker (2002), Variability of absorption and optical properties of key aerosol types observed in worldwide locations. *J. Atmos. Sci.*, *59*, 590-608.

Dubovik, O., A. Sinyuk, T. Lapyonok, B. N. Holben, M. Mishchenko, P. Yang, T. F. Eck, H. Volten, O. Muñoz, B. Veihelmann, W. J. van der Zande, J.-F. Leon, M. Sorokin, and I. Slutsker (2006), Application of spheroid models to account for aerosol particle nonsphericity in remote sensing of desert dust, *J. Geophys. Res.*, *111*, D11208, doi:10.1029/2005JD006619.

Fraser, R. S., and Y. J. Kaufman (1985), The relative importance of aerosol scattering and absorption in remote sensing, *IEEE Trans. Geosci. Remote Sens. GE-23*, 625-633.

Hansen, J., M. Sato, and R. Ruedy (1997), Radiative forcing and climate response, *J. Geophys. Res.*, *102*, 6831–6864, doi:10.1029/96JD03436.

Haywood, J. M., and K. P. Shine (1997), Multi-spectral calculations of the radiative forcing of tropospheric sulphate and soot aerosols using a column model, *Quart. J. Roy. Meteor. Soc.*, *123*, 1907-1930.

Haywood, J. M., S. R. Osborne, and S. J. Abel (2004), The effect of overlying absorbing aerosol layers on remote sensing retrievals of cloud effective radius and cloud optical depth, *Q. J. R. Meteorol. Soc.*, *130*, 779-800.

Hobbs, P. V., J. S. Reid, R. A. Kotchenruther, R. J. Ferek, and R. Weiss (1997), Direct radiative forcing by smoke from biomass burning, *Science*, *275*, 1776–1778.

Holben, B. N., T. F. Eck, I. Slutsker, D. Tanre´, J. P. Buis, A. Setzer, E. Vermote, J. A. Reagan, Y. J. Kaufman, T. Nakajima, F. Lavenu, I. Jankowiak, and A. Smirnov (1998), AERONET—A federated instrument network and data archive for aerosol characterization, *Remote Sens. Environ.*, *66*, 1– 16.

Hu, Y., M. Vaughan, Z. Liu, K. Powell, and S. Rodier (2007), Retrieving optical depths and lidar ratios for transparent layers above opaque water clouds from CALIPSO lidar measurements, *IEEE Trans. Geosci. Remote Sens. Lett.*, *4*, 523–526.

Hu, Y., D. Winker, M. Vaughan, B. Lin, A. Omar, C. Trepte, D. Flittner, P. Yang, S. L. Nasiri, B. Baum, R. Holz, W. Sun, Z. Liu, Z. Wang, S. Young, K. Stamnes, J. Huang, and R. Kuehn (2009), CALIPSO/CALIOP cloud phase discrimination algorithm, *J. Atmos. Oceanic Technol.*, *26*, 2293–2309, http://dx.doi.org/10.1175/2009JTECHA1280.1.

Hubanks, P., M. D. King, S. Platnick, and R. Pincus (2008), *MODIS Atmosphere L3 Gridded Product Algorithm Theoretical Basis Document*, ATBD Reference Number: ATBD-MOD-30.

Ichoku, C., D. A. Chu, S. Mattoo, Y. J. Kaufman, L. A. Remer, D. Tanre´, I. Slutsker, and B. N. Holben (2002), A spatio-temporal approach for global validation and analysis of MODIS aerosol products, *Geophys. Res. Lett.*, *29(12)*, doi:10.1029/2001GL013206.

Intergovernmental Panel of Climate Change (IPCC) (2013), *Climate Change 2013: The Physical Science Basis. Contribution of Working Group I to the Fifth Assessment Report of the Intergovernmental Panel on Climate Change*, edited by: Stocker, T. F., Qin, D., Plattner, G.-K., Tignor, M., Allen, S. K., Boschung, J., Nauels, A., Xia, Y., Bex, V., and Midgley, P. M., 1535pp., Cambridge University Press, Cambridge, United Kingdom and New York, doi:10.1017/CBO9781107415324.

Kalnay, E., M. Kanamitsu, R. Kistler, W. Collins, D. Deaven, L. Gandin, M. Iredell, S. Saha, G. White, J. Woollsen, Y. Zhu, M. Chelliah, W. Ebisuzaki, W. Higgins, J. Janowiak, K. C. Mo, C. Ropelewski, J. Wang, A. Leetmaa, R. Reynolds, R. Jenne, and D. Joseph (1996), The NCEP/NCAR 40-year reanalysis project, *Bull. Amer. Meteor. Soc.*, *77*, 437-471.

Kaufman, Y.J., D. Tanre, O. Dubovik, A. Karnieli, and L.A. Remer (2001), Absorption of sunlight by dust as inferred from satellite and ground-based remote sensing, *Geophys. Res. Lett.*, *28*, 1479-1482.

Kaufman, Y. J., L. A. Remer, D. Tanr´e, R.-R. Li, R. Kleidman, S. Mattoo, R. Levy, T. Eck, B. N. Holben, C. Ichoku, J. Martins, and I. Koren (2005), A critical examination of the residual cloud contamination and diurnal sampling effects on MODIS estimates of aerosol over ocean, *IEEE Trans. on Geoscience & Remote Sensing*, *43(12)*, 2886–2897.

Keil, A., and J. M. Haywood (2003), Solar radiative forcing by biomass burning aerosol particles during SAFARI 2000: A case study based on measured aerosol and cloud properties, *J. Geophys. Res.*, *108*, 8467, doi:10.1029/2002JD002315.

Kim, D. and V. Ramanathan (2008), Solar radiation budget and radiative forcing due to aerosols and clouds, *J. Geophys. Res.*, *113*, D02203, doi:10.1029/2007JD008434.

Kinne, S., M. Schulz, C. Textor, S. Guibert, Y. Balkanski, S. E. Bauer, T. Berntsen, T. F. Berglen, O. Boucher, M. Chin, W. Collins, F. Dentener, T. Diehl, R. Easter, J., Feichter, D. Fillmore, S. Ghan, P. Ginoux, S. Gong, A. Grini, J. Hendricks, M. Herzog, L. Horowitz, I. Isaksen, T., Iversen, A. Kirkevåg, S. Kloster, D. Koch, J. E. Kristjansson, M. Krol, A. Lauer, J. F. Lamarque, G. Lesins, X. Liu, U. Lohmann, V. Montanaro, G. Myhre, J. Penner, G. Pitari, S. Reddy, O. Seland, P. Stier, T. Takemura, and X. Tie (2006), An AeroCom initial assessment – optical properties in aerosol component modules of global models, *Atmos. Chem. Phys.*, *6*, 1815-1834, doi:10.5194/acp-6-1815-2006.

Kinne, S., D. O'Donnel, P. Stier, S. Kloster, K. Zhang, H. Schmidt, S. Rast, M. Giorgetta, T. F. Eck, and B. Stevens (2013), MAC-v1: A new global aerosol climatology for climate studies, *J. Adv. Model. Earth Syst.*, *5*, 704–740, doi:10.1002/jame.20035.

Kittaka, C., D. M. Winker, M. A. Vaughan, A. Omar, and L. A. Remer (2011), Intercomparison of column aerosol optical depths from CALIPSO and MODIS-Aqua, *Atmos. Meas. Tech.*, *4*, 131-141, doi:10.5194/amt-4-131-2011.

Kneizys P. X., E. P. Shettle, L. W. Abreu, J. H. Chetwynd, G. P. Anderson, W. O. Gallery, J. E. A. Selby, and S. A. Clough (1988), Users Guide to LOWTRAN 7, *Rep. AFGL-TR-88-0177, Bedford, MA: Air Force Geophys. Lab.*.

Levy, R. C., L. A. Remer, S. Mattoo, E. F. Vermote, and Y. J. Kaufman (2007), Second-generation operational algorithm: Retrieval of aerosol properties over land from inversion of Moderate Resolution Imaging Spectroradiometer spectral reflectance, *J. Geophys. Res.*, *112*, D13211, doi:10.1029/2006JD007811.

Levy, R. C., L. A. Remer, R. G. Kleidman, S. Mattoo, C. Ichoku, R. Kahn, and T. F. Eck (2010), Global evaluation of the Collection 5 MODIS dark-target aerosol products over land, *Atmos. Chem. Phys.*, *10*, 10399–10420, doi:10.5194/acp-10-10399-2010.

Li, Y., R. Yu, Y. Xu, and X. Zhang (2004), Spatial distribution and seasonal variation of cloud over China based on ISCCP data and surface observations, *J. Meteor. Soc. Japan, 82*, 761–773.

Liu, X., J. E. Penner, B. Das, D. Bergmann, J. M. Rodriguez, S. Strahan, M. Wang, and Y. Feng (2007), Uncertainties in global aerosol simulations: Assessment using three meteorological data sets, *J. Geophys. Res.*, *112*, D11212, doi:10.1029/2006JD008216.

Liu, Z., M. A. Vaughan, D. M. Winker, C. Kittaka, B. J. Getzewich, R. E. Kuehn, A. Omar, K. Powell, C. R. Trepte, and C. A. Hostetler (2009), The CALIPSO lidar cloud and aerosol discrimination: Version 2 algorithm and initial assessment of performance. *J. Atmos. Oceanic Technol., 26*, 1198–1213.

Liu, Z., R. Kuehn, M. Vaughan, D. Winker, A. Omar, K. Powell, C. Trepte, Y. Hu, and C. Hostetler (2010), The CALIPSO cloud and aerosol discrimination: Version 3 algorithm and test results, *25th International Laser Radar Conference (ILRC)*, St. Petersburg, Russia, ISBN 978-5-94458-109-9.

Ma, X., F. Yu, and G. Luo (2012), Aerosol direct radiative forcing based on GEOS-Chem-APM and uncertainties, *Atmos. Chem. Phys.*, *12*, 5563-5581, doi:10.5194/acp-12-5563-2012.

Meyer, K., S. Platnick, L. Oreopoulos, and D. Lee (2013), Estimating the direct radiative effect of absorbing aerosols overlying marine boundary layer clouds in the southeast Atlantic using MODIS and CALIOP, *J. Geophys. Res. Atmos.*, *118*, 4801–4815, doi:10.1002/jgrd.50449.

Myhre, G. (2009), Consistency between satellite-derived and modeled estimates of the direct aerosol effect, *Science*, *325*, 187–190.

Myhre, G., B. H. Samset, M. Schulz, Y. Balkanski, S. Bauer, T. K. Berntsen, H. Bian, N. Bellouin, M. Chin, T. Diehl, R. C. Easter, J. Feichter, S. J. Ghan, D. Hauglustaine, T. Iversen, S. Kinne, A. Kirkevåg, J.-F. Lamarque, G. Lin, X. Liu, M. T. Lund, G. Luo, X. Ma, T. van Noije, J. E. Penner, P. J. Rasch, A. Ruiz, Ø. Seland, R. B. Skeie, P. Stier, T. Takemura, K. Tsigaridis, P. Wang, Z. Wang, L. Xu, H. Yu, F. Yu, J.-H. Yoon, K. Zhang, H. Zhang, and C. Zhou (2013), Radiative forcing of the direct aerosol effect from AeroCom Phase II simulations, *Atmos. Chem. Phys*., *13*, 1853-1877, doi:10.5194/acp-13-1853-2013.

Nakajima, T. and M. Tanaka (1983), Effect of wind-generated waves on the transfer of solar radiation in the atmosphere-ocean system, *J. Quant. Spectrosc. Radiat. Transfer*, *29*, 521–537.

Nakajima, T. and M. Tanaka (1986), Matrix formulations for the transfer of solar radiation in a plane-parallel scattering atmosphere, *J. Quant. Spectrosc. Radiat. Transfer*, *35*, 13–21.

Nakajima, T., and M. Tanaka (1988), Algorithms for radiative intensity calculations in moderately thick atmospheres using a truncation approximation, *J. Quant. Spectrosc. Radiat. Transfer*, *40*, 51-69.

Nakajima, T., G. Tonna, R. Rao, Y. Kaufman, and B. Holben (1996), Use of sky brightness measurements from ground for remote sensing of particulate polydispersions. *App. Opt., 35*, 2672-2686.

Nakajima, T., S.-C. Yoon, V. Ramanathan, G.-Y. Shi, T. Takemura, A. Higurashi, T. Takamura, K. Aoki, B.-J. Sohn, S.-W. Kim, H. Tsuruta, N. Sugimoto, A. Shimizu, H. Tanimoto, Y. Sawa, N.-H. Lin, C.-T. Lee, D. Goto, and N. Schutgens (2007), Overview of the Atmospheric Brown Cloud East Asian Regional Experiment 2005 and a study of the aerosol direct radiative forcing in east Asia, *J. Geophys. Res.*, *112*, D24S91, doi:10.1029/2007JD009009.

Omar, A. H., D. M. Winker, C. Kittaka, M. A. Vaughan, Z. Liu, Y. Hu, C. R. Trepte, R. R. Rogers, R. A. Ferrare, K.-P. Lee, R. E. Kuehn, and C. A. Hostetler (2009), The CALIPSO automated aerosol classification and lidar ratio selection algorithm, *J. Atmos. Oceanic Technol.*, *26*, 1994–2014.

Omar, A. H., D. M. Winker, J. L. Tackett, D. M. Giles, J. Kar, Z. Liu, M. A.

Vaughan, K. A. Powell, and C. R. Trepte (2013), CALIOP and AERONET aerosol optical depth comparisons: One size fits none, *J. Geophys. Res. Atmos.*, *118*, 4748–4766, doi:10.1002/jgrd.50330.

Platnick, S., M. D. King, S. A. Ackerman, W. P. Menzel, B. A. Baum, J. C. Riedi, and R. A. Frey (2003), The MODIS cloud products: Algorithms and examples from Terra, *IEEE Trans. Geosci. Remote Sens.*, *41*, 459–473.

Powell, K. A., M. A. Vaughan, R. R. Rogers, R. E. Kuehn, W. H. Hunt, K.-P. Lee, and T. D. Murray (2010), The CALIOP 532- nm channel daytime calibration: Version 3 algorithm, *Proceedings of the 25th International Laser Radar Conference*, 1367–1370, ISBN 978-5-94458-109-9.

Rayner, N. A., D. E. Parker, E. B. Horton, C. K. Folland, L. V. Alexander, D. P. Rowell, E. C. Kent, and A. Kaplan (2003), Global analyses of sea surface temperature, sea ice, and night marine air temperature since the late nineteenth century, *J. Geophys. Res.*, *108*, 4407, doi:10.1029/2002JD002670, D14.

Redemann, J., M. A. Vaughan, Q. Zhang, Y. Shinozuka, P. B. Russell, J. M. Livingston, M. Kacenelenbogen, and L. A. Remer (2012), The comparison of MODIS-Aqua (C5) and CALIOP (V2 &V3) aerosol optical depth, *Atmos. Chem. Phys.*, *12*, 3025–3043, doi:10.5194/acp-12-3025-2012.

Remer, L. A., D. Tanré, Y. J. Kaufmann, C. Ichoku, S. Mattoo, R. Levy, D. A. Chu, B. Holben, O. Dubovik, A. Smirnov, J. V. Martins, R.-R. Li, and Z. Ahmad (2002), Validation of MODIS aerosol retrieval over ocean, *Geophys. Res. Lett.*, *29(12)*, doi:10.1029/2001GL013204.

Remer, L. A., Y. J. Kaufman, D. Tanré, S. Mattoo, D. A. Chu, J. V. Martins, R.-R. Li, C. Ichoku, R. C. Levy, R. G. Kleidman, T. F. Eck, E. Vermote, and B. N. Holben (2005), The MODIS aerosol algorithm, products, and validation, *J. Atmos. Sci.*, *62*, 947–973. doi: http://dx.doi.org/10.1175/JAS3385.1.

Remer, L. A., R. G. Kleidman, R. C. Levy, Y. J. Kaufman, D. Tanré, S. Mattoo, J. V. Martins, C. Ichoku, I. Koren, H. Yu and B. N. Holben (2008), Global aerosol climatology from the MODIS satellite sensors, *J. Geophys. Res.*, *113*, D14S07, doi:10.1029/2007JD009661.

Rienecker, M. M., M. J. Suarez, R. Gelaro, R. Todling, J. Bacmeister, E. Liu, M. G. Bosilovich, S. D. Schubert, L. Takacs, G.-K. Kim, S. Bloom, J. Chen, D. Collins, A. Conaty, A. da Silva, W. Gu, J. Joiner, R. D. Koster, R. Lucchesi, A. Molod, T. Owens, S. Pawson, P. Pegion, C. R. Redder, R. Reichle, F. R. Robertson, A. G. Ruddick, M. Sienkiewicz, and J. Woollen (2011), MERRA: NASA's Modern-Era Retrospective Analysis for Research and Applications, *J. Climate*, *24*, 3624–3648.

doi: http://dx.doi.org/10.1175/JCLI-D-11-00015.1.

Roesch, A., C. Schaaf, and F. Gao (2004), Use of Moderate-Resolution Imaging Spectroradiometer bidirectional reflectance distribution function products to enhance simulated surface albedos, *J. Geophys. Res.*, *109*, D12105, doi:10.1029/2004JD004552.

Román, M. O., C. B. Schaaf, P. Lewis, F. Gao, G. P. Anderson, J. L. Privette, A. H. Strahler, C. E. Woodcock, M. Barnsley (2010), Assessing the coupling between surface albedo derived from MODIS and the fraction of diffuse skylight over spatially-characterized landscapes, *Remote Sensing of Environment*, *114*, 738-760.

Rothman, L.S., D. Jacquemart, A. Barbe, D.C. Benner, M. Birk, L.R. Brown, M.R. Carleer, C. Chackerian, K. Chance, L.H. Coudert, V. Dana, V.M. Devi, J.M. Flaud, R.R. Gamache, A. Goldman, J.M. Hartmann, K.W. Jucks, A.G. Maki, J.Y. Mandin, S.T. Massie, J. Orphal, A. Perrin, C.P. Rinsland, M.A. Smith, J. Tennyson, R.N. Tolchenov, R.A. Toth, J. Vander Auwera, P. Varanasi, and G. Wagner (2005), The HITRAN 2004 molecular spectroscopic database, *J. Quant. Spectrosc. Radiat. Transfer*, *96*, 139–204. DOI: 10.1016/j.jqsrt.2004.10.008.

Ruggaber, A., R. Dlugi, and T. Nakajima (1994), Modelling of radiation quantities and photolysis frequencies in the troposphere, *J. Atmos. Chem.*, *18*, 171-210.

Satheesh, S. K., S. Deepshikha and J. Srinivasan (2006), Impact of dust aerosol on Earth-atmosphere clear-sky albedo and its short wave radiative forcing over Africa and Arabian regions. *Int. J. Remote Sens.*, *27*, 1691-1706.

Schaaf, C. B., F. Gao, A. H. Strahler, W. Lucht, X. Li, T. Tsang, N. C. Strugnell, X. Zhang, Y. Jin, J.-P. Muller, P. Lewis, M. Barnsley, P. Hobson, M. Disney, G. Roberts, M. Dunderdale, C. Doll, R. P. d'Entremont, B. Hu, S. Liang, J. L. Privette, and D. Roy (2002), First operational BRDF, albedo nadir reflectance products from MODIS, *Remote Sens. Environ.*, *83*, 135–148.

Schulz, M., C. Textor, S. Kinne, Y. Balkanski, S. E. Bauer, T. Berntsen, T. Berglen, O. Boucher, F. Dentener, A. Grini, S. Guibert, T. Iversen, D. Koch, A. Kirkev°ag, X. Liu, V. Montanaro, G. Myhre, J. Penner, G. Pitari, S. Reddy, Ø. Seland, P. Stier, and T. Takemura (2006), Radiative forcing by aerosols as derived from the AeroCom present-day and pre-industrial simulations, *Atmos. Chem. Phys., 6*, **5225–5246.**

Sekiguchi, M., and T. Nakajima (2008), A k-distribution-based radiation code and its computational optimization for an atmospheric general circulation model. *J. Quant. Spectrosc. Radiat. Transfer*, *109*, 2779–2793.

Sutherland, R. A., and R. K. Khanna (1991), Optical properties of organic-based aerosols produced by burning vegetation, *Aerosol Sci, Techonol.*, *14*, 331-342.

Takata, K., S. Emori, and T. Watanabe (2003), Development of the minimal advanced treatments of surface interaction and runoff, *Global Planet. Change*, 38, 209–222.

Takemura, T., H. Okamoto, Y. Maruyama, A. Numaguti, A. Higurashi, and T. Nakajima (2000), Global three-dimensional simulation of aerosol optical thickness distribution of various origins, *J. Geophys. Res.*, *105*, 17,853– 17,873.

Takemura, T., T. Nakajima, O. Dubovik, B. N. Holben, and S. Kinne (2002), Single scattering albedo and radiative forcing of various aerosol species with a global three-dimensional model, *J. Clim.*, *15*, 333–352.

Takemura, T., T. Nozawa, S. Emori, T. Y. Nakajima, and T. Nakajima (2005), Simulation of climate response to aerosol direct and indirect effects with aerosol transport-radiation model, *J. Geophys. Res.*, *110*, D02202, doi:10.1029/ 2004JD005029.

Takemura, T., M. Egashira, K. Matsuzawa, H. Ichijo, R. O'ishi, and A. Abe-Ouchi (2009), A simulation of the global distribution and radiative forcing of soil dust aerosols at the Last Glacial Maximum, *Atmos. Chem. Phys.*, *9*, 3061-3073, doi:10.5194/acp-9-3061-2009.

Tang, I. N., and H. R. Munkelwitz (1994), Water activities, densities, and refractive indices of aqueous sulfates and sodium nitrate droplets of atmospheric importance, *J. Geophys. Res.*, *99*, 18,801– 18,808.

Textor, C., M. Schulz, S. Guibert, S. Kinne, Y. Balkanski, S. Bauer, T. Berntsen, T. Berglen, O. Boucher, M. Chin, F. Dentener, T. Diehl, R. Easter, H. Feichter, D. Fillmore, S. Ghan, P. Ginoux, S. Gong, A. Grini, J. Hendricks, L. Horowitz, P. Huang, I. Isaksen, I. Iversen, S. Kloster, D. Koch, A. Kirkevåg, J. E. Kristjansson, M. Krol, A. Lauer, J. F. Lamarque, X. Liu, V. Montanaro, G. Myhre, J. Penner, G. Pitari, S. Reddy, Ø. Seland, P. Stier, T. Takemura, and X. Tie (2006), Analysis and quantification of the diversities of aerosol life cycles within AeroCom, *Atmos. Chem. Phys.*, *6*, 1777-1813, doi:10.5194/acp-6-1777-2006.

Thomson, A. M., K. V. Calvin, S. J. Smith, G. P. Kyle, A. Volke, P. Patel, S. Delgado-Arias, B. Bond-Lamberty, M. A. Wise, L. E. Clarke, and J. A. Edmonds (2011), RCP4.5: a pathway for stabilization of radiative forcing by 2100, *Clim. Change*, *109*, 77–94.

Twomey, S. (1977), Influence of pollution on shortwave albedo of clouds. *J. Atmos. Sci.*, *34*, 1149–1152.

Vaughan, M., K. Powell, R. Kuehn, S. Young, D. Winker, C. Hostetler, W. Hunt, Z. Liu, M. McGill, and B. Getzewich (2009), Fully automated detection of cloud and aerosol layers in the CALIPSO lidar measurements, *J. Atmos. Oceanic Technol.*, *26*, 2034–2050.

Vaughan, M., R. Kuehn, J. Tackett, R. Rogers, Z. Liu, A. Omar, B. Getzewich, K. Powell, Y. Hu, S. Young, M. Avery, D. Winker, and C. Trepte (2010), Strategies for improved CALIPSO aerosol optical depth estimates, *Proceedings of the 25th International Laser Radar Conference*, 1340–1343, ISBN 978-5-94458-109-9.

Watanabe, M., S. Emori, M. Satoh, and H. Miura (2009), A PDF based hybrid prognostic cloud scheme for general circulation models, *Climate Dyn.*, *33*, 795–816, doi:10.1007/s00382-008-0489-0.

Watanabe, M., T. Suzuki, R. O'ishi, Y. Komuro, S. Watanabe, S. Emori, T. Takemura, M. Chikira, T. Ogura, M. Sekiguchi, K. Takata, D. Yamazaki, T. Yokohata, T. Nozawa, H. Hasumi, H. Tatebe, and M. Kimoto (2010), Improved climate simulation by MIROC5: mean states, variability, and climate sensitivity, *J. Climate*, *23*, 6312–6335. doi: http://dx.doi.org/10.1175/2010JCLI3679.1.

Wilson, D. R., and S. P. Ballard (1999), A microphysically based precipitation scheme for the UK Meteorological Office unified model, *Quart. J. Roy. Meteor. Soc.*, *125*, 1607–1636.

Winker, D. M., M. Vaughan, A. Omar, Y. Hu, K. Powell, Z. Liu, W. Hunt, and S. A. Young (2009), Overview of the CALIPSO mission and CALIOP data processing algorithms, *J. Atmos. Oceanic Technol.*, *26*, 2310-2323.

Winker, D. M., J. Pelon, J. A. Coakley Jr., S. A. Ackerman, R. J. Charlson, P. R. Colarco, P. Flamant, Q. Fu, R. M. Hoff, C. Kittaka, T. L. Kubar, H. Le Treut, M. P. McCormick, G. Mégie, L. Poole, K. Powell, C. Trepte, M. A. Vaughan, and B. A. Wielicki (2010), The CALIPSO Mission: A global 3D view of aerosols and clouds, *Bull. Amer. Meteor. Soc.*, *91*, 1211-1229.

Winker, D. M., J. L. Tackett, B. J. Getzewich, Z. Liu, M. A. Vaughan, and R. R. Rogers (2013), The global 3-D distribution of tropospheric aerosols as characterized by CALIOP, *Atmos. Chem. Phys.*, *13*, 3345-3361, doi:10.5194/acp-13-3345-2013.

Yoshida, M., and H. Murakami (2008), Dust absorption averaged over the Sahara inferred from moderate resolution imaging spectroradiometer, *Appl. Opt.*, *47*, 1995-2003.

Young, S. A., and M. A. Vaughan (2009), The retrieval of profiles of particulate extinction from Cloud Aerosol Lidar Infrared Pathfinder Satellite Observations (CALIPSO) data: Algorithm description, *J. Atmos. Oceanic Technol.*, *26*, 1105-1119, doi:10.1175/2008 JTECHA1221.1.

Yu, H., R. E. Dickinson, M. Chin, Y. J. Kaufman, M. Zhou, L. Zhou, Y. Tian, O.

Dubovik, and B. N. Holben (2004), Direct radiative effect of aerosols as determined from a combination of MODIS retrievals and GOCART simulations, *J. Geophys. Res.*, *109*, D03206, doi:10.1029/2003JD003914.

Yu, H., Y. J. Kaufman, M. Chin, G. Feingold, L. A. Remer, T. L. Anderson, Y. Balkanski, N. Bellouin, O. Boucher, S. Christopher, P. DeCola, R. Kahn, D. Koch, N. Loeb, M. S. Reddy, M. Schulz, T. Takemura, and M. Zhou (2006), A review of measurement-based assessments of the aerosol direct radiative effect and forcing, *Atmos. Chem. Phys.*, *6*, 613-666, doi:10.5194/acp-6-613-2006.

Zhang, K., D. O'Donnell, J. Kazil, P. Stier, S. Kinne, U. Lohmann, S. Ferrachat, B. Croft, J. Quaas, H. Wan, S. Rast, and J. Feichter (2012), The global aerosol-climate model ECHAM-HAM, version 2: sensitivity to improvements in process representations, *Atmos. Chem. Phys*., 12, 8911-8949, doi:10.5194/acp-12-8911-2012.

Zhang, Z., K. Meyer, S. Platnick, L. Oreopoulos, D. Lee, and H. Yu (2014), A novel method for estimating shortwave direct radiative effect of above-cloud aerosols using CALIOP and MODIS data, *Atmos. Meas. Tech.*, 7, 1777-1789, doi:10.5194/amt-7-1777-2014.